

# Quantum electrodynamics near photonic Weyl points

Iñaki García-Elcano,<sup>1</sup> Alejandro González-Tudela,<sup>2,\*</sup> and Jorge Bravo-Abad<sup>1,†</sup>

<sup>1</sup>*Departamento de Física Teórica de la Materia Condensada and Condensed Matter Physics Center (IFIMAC),  
Universidad Autónoma de Madrid, E-28049 Madrid, Spain*

<sup>2</sup>*Instituto de Física Fundamental IFF-CSIC, Calle Serrano 113b, Madrid 28006, Spain*

Weyl photons appear when two three-dimensional photonic bands with linear dispersion are degenerate at a single momentum point, labeled as Weyl point. These points have remarkable properties such as being robust topological monopoles of Berry curvature as well as an associated vanishing density of states. Here, we study the quantum optical consequences of such topological Weyl photons by characterizing the individual and collective dynamics of quantum emitters close to resonance with these points. Using an exact non-perturbative treatment, we predict the development of non-exponential decay dynamics due to the emergence of localized photonic states around the emitters. We find that these bound states, whose wavefunction displays power-law spatial decay, can mediate coherent and topological long-range interactions when many emitters exchange energy through Weyl photons. Furthermore, by exploiting the topological protection of Weyl points, we provide a recipe to tune the range of the mediated interactions while keeping their power-law nature, something not possible in any other photonic platform. Thus, Weyl photons enable coherent, tunable, long-range interactions between emitters, and therefore can become a very valuable platform in the context of quantum simulation.

Bridging topology and photonics opens exciting avenues to control and mold the flow of light in exotic ways [1–3]. In three-dimensions (3D), a remarkable paradigm of such effects are the photonic counterpart of Weyl fermions [4]. Weyl photonic excitations appear in structures that break time-parity symmetry, leading to the emergence of the so-called photonic Weyl points. These are points in reciprocal space in which two linearly dispersive bands touch creating a singular band-gap, much in the same way as occurs in Dirac two-dimensional systems [5]. However, a key difference with respect to them is that Weyl points are topologically protected: a Weyl point can only be annihilated when it meets another Weyl point with opposite chirality [6], providing them important advantages such as robustness to disorder [7, 8]. These unique properties motivated a race for their experimental observation, which was first achieved in double-gyroid photonic crystals [9], and then followed by many other proposals and demonstrations [10–24].

Even though the properties of Weyl photons themselves have been mostly established, their impact on light-matter interactions remains largely unexplored. An intriguing question arising in this context is whether the unique features of Weyl points translate into unconventional quantum optical behaviour, like it happens with standard photonic band-gaps [25–28]. In this letter, we address this question by studying the individual and collective dynamics of quantum emitters (QEs) interacting with a photonic Weyl environment, and predict that they lead to several distinctive phenomena. First, we show the development of non-exponential decay dynamics of a single emitter, even if the bath density of states at their transition frequency is strictly zero and smooth around it. This occurs because a photonic bound state forms around the emitters, which we also show to have fundamentally different properties compared to those appearing in standard photonic band-gaps [25–28]. We show that these bound states display a power-law spatial decay,  $1/d^\gamma$ , whose exponent  $\gamma$  can be tuned between  $\gamma \in [3/2, 3]$  by exploiting the topolog-

ical robustness of the Weyl points. Furthermore, we show that these tunable bound states are especially relevant when many emitters couple to a Weyl photonic bath, because they mediate decoherence-free, tunable, and long-range interactions between them. Thus, Weyl photonic platforms stand as very unique systems to develop applications that harness long-range emitters interactions, such as the generation of long-distance entanglement [29], creation of large optical nonlinearities [30], or the quantum simulation of long-range interacting many-body physics [31–37]. In addition, this work opens us a fundamentally new in direction in the emerging area of topological quantum optics [38–40].

To illustrate our findings we use the discrete photonic lattice sketched in Fig. 1(a), consisting of a nearest-neighbour staggered hopping model (of lattice constant  $a$  and hopping strength  $J$ ). Such system defines a bipartite lattice of localized photonic modes ( $A/B$  sublattices), whose Hamiltonian reads (taking  $\hbar = 1$ ) [41, 42]:

$$H_B = J \sum_{\mathbf{r}} [(-1)^{x+y} (c_{\mathbf{r}}^\dagger c_{\mathbf{r}+a\hat{z}} - c_{\mathbf{r}}^\dagger c_{\mathbf{r}+a\hat{y}}) + c_{\mathbf{r}}^\dagger c_{\mathbf{r}+a\hat{x}} + \text{H.c.}] + M \sum_{\mathbf{r}} (-1)^{x+y} c_{\mathbf{r}}^\dagger c_{\mathbf{r}}, \quad (1)$$

where  $c_{\mathbf{r}}^\dagger$  ( $c_{\mathbf{r}}$ ) is the creation (annihilation) operator of the photonic mode at the position  $\mathbf{r}$ , and where we are already taking the energy of the photonic modes at each site as the energy reference of the problem. In Eq. (1) we also assume that the system features a tunable sublattice frequency offset  $M$ , so that the frequencies of the photonic modes in sites  $A$  and  $B$  are  $+M$  and  $-M$ , respectively.

By imposing periodic boundary conditions, and by writing  $H_B$  in  $\mathbf{k}$ -space,  $H_B$  can be readily diagonalized [43], resulting in two energy bands  $\pm\omega(\mathbf{k})$ . In Fig. 1(b) we plot a two dimensional cut of  $\pm\omega(k_x, 0, k_z)$  computed for  $M = 0$ , where it is clear the emergence of four Weyl points at  $\{k_x a, k_z a\} = \{\pm\pi/2, \pm\pi/2\}$  at frequency  $\omega_W = 0$ . Figure 1(c) displays the corresponding density of states  $D(\omega)$ , which shows the expected quadratic dependence in the vicinity of the Weyl point.

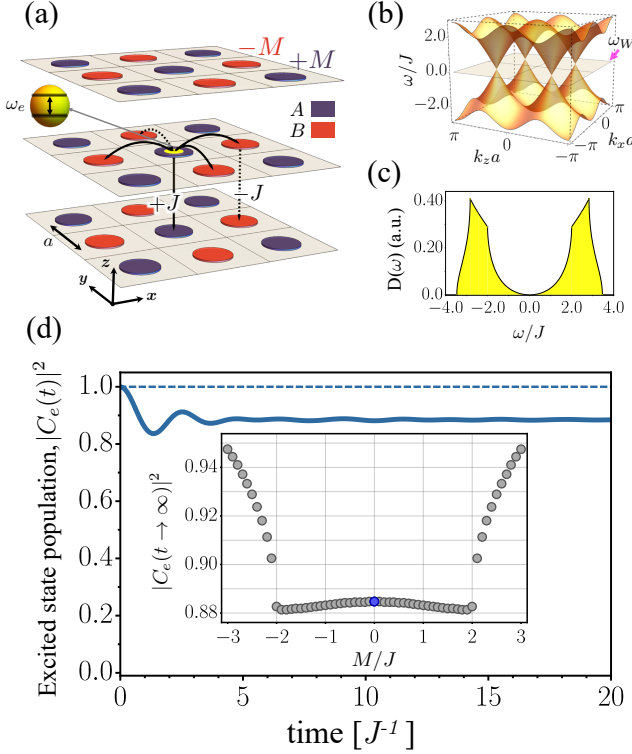


Figure 1. (a) Schematics of the analyzed system. Blue (red) shallow cylinders represent sublattice A (B) of the system. Solid and dashed arrows correspond to positive and negative first-neighbour hoppings,  $J$ , respectively.  $M$  denotes the sublattice frequency offset, whereas  $a$  is the lattice constant. (b) Dispersion relation of the lattice shown in (a), for  $M = 0$  and  $k_y = 0$ .  $\omega_W$  marks the frequency of the Weyl points. (c) Density of states,  $D(\omega)$ , associated to the lattice shown in (a). (d) Dynamics of the quantum emitter's excited state population,  $|C_e(t)|^2$ , calculated for  $\omega_e = \omega_W$  and  $M = 0$ . Solid and dashed lines correspond to exact and perturbative approaches, respectively. Inset shows  $|C_e(t \rightarrow \infty)|^2$  versus  $M$  (the blue dot marks the case considered in the main figure). For  $M \neq 0$  a finite detuning  $\omega_e - \omega_W = \Delta_c$  is assumed. All displayed results correspond to  $g = 0.5J$ .

Additional non-analytic spectral regions, such as band-edges and Van Hove singularities, appear in  $D(\omega)$ , which although will not be the focus of this work, can also be source of non-trivial quantum dynamics [44].

As mentioned, the main motivation of this work is to study the quantum electrodynamical features of Weyl photons. For that, we start by considering the case of a single QE, described as a two-level system ( $\{|g\rangle, |e\rangle\}$ ), whose optical transition (with detuning  $\Delta$  with respect to the Weyl point) couples to such type of photons. The full quantum electrodynamical Hamiltonian of that problem reads  $H = H_e + H_B + H_I$ , where  $H_e = \Delta \sigma_{ee}$  describes the intrinsic QE dynamics, and  $H_I$  is the light-matter interaction term,  $H_I = g(c_r \sigma_{eg} + \text{H.c.})$  (the parameter  $g$  is the light-matter interaction strength to the  $c_r$  mode [45]). Throughout this work we use the notation  $\sigma_{\mu\nu} = |\mu\rangle\langle\nu|$  for the *spin operator* of the QE.

The first relevant situation in this context is the so-called

spontaneous emission dynamics problem [26]. There, one assumes the QE is initially excited with no photons in the bath ( $|\text{vac}\rangle_B$ ), and study the decay of its population ( $|C_e(t)|^2$ ) due to the interaction with the bath. Perturbative treatments, like Fermi's golden rule or Markov approximation [46] (which assume a smooth density of states around the QE frequencies), predict an exponential decay of the population at a rate proportional to the density of states at the QE frequency, i.e.,  $\Gamma_M \propto g^2 D(\Delta)$ . Since the Weyl photonic bath shows  $D(\omega) \propto \omega^2$  for  $|\omega| \ll J$  (see Fig. 1(c)), one expects to see a no decay dynamics as the one plotted in dashed line of Fig. 1(d) when the QE frequency exactly matches the Weyl point. However, when calculating *exactly* the dynamics (see details in [43]), as plotted in the solid line of Fig. 1(c) for a situation with  $g = 0.5J$  and  $\Delta = 0$ , we observe the first surprising difference: the QE features first an initial decay at short times, followed by a set of oscillations, after which it settles down to a value that we found to be [43]  $|C_e(t \rightarrow \infty)| \approx 1/[1 + 0.25(g/J)^2]$ . Thus, perturbative predictions are only approximately recovered when  $g/J \ll 1$ . Previous works in conventional photonic band-gaps have interpreted this type of *fractional decay* [26] as the signature of a light-matter bound state associated to the presence of non-analytic gapped regions of  $D(\omega)$  in the close vicinity of QE frequency. Remarkably, in this work we obtain a similar non-Markovian decay near the Weyl point, which lies in the middle of a smooth spectrum.

Despite the similarities of the obtained QE dynamics with that found in standard photonic band-gaps, the emergent bound state (BS) giving rise to the steady-state population  $|C_e(t \rightarrow \infty)|^2$  shown in Fig. 1(d) displays very different features from the ones appearing in these environments. To evidence this, we calculate the exact bound state wavefunction in the single-excitation subspace  $|\psi_{BS}\rangle = (C_e^{BS} \sigma_{eg} + \sum_r C_r^{BS} c_r^\dagger) |g\rangle \otimes |\text{vac}\rangle_B$  using the secular equation  $H |\psi_{BS}\rangle = E_{BS} |\psi_{BS}\rangle$ . In particular, we focus on the spatial distribution of the BS photonic component ( $C_r^{BS}$ ), which we plot in Fig. 2 for several illustrative parameters for a lattice of size  $20 \times 20 \times 20$  (in all cases  $|C_r^{BS}|$  has been normalized by  $(g/J)|C_e(t \rightarrow \infty)|$ ). For  $\Delta = 0$  (and  $M = 0$ ), we find that the BS energy is  $E_{BS} = 0$ , and that its photonic component localizes around the QE mostly in an isotropic fashion with a power-law spatial decay  $\sim 1/d^2$ . This is clearly visualized in Figs. 2(a) and (d), which display, respectively, the 3D spatial distribution of  $|C_r^{BS}|$  near the QE and its dependence along the  $xy$ - and  $z$ -directions. This type of spatial decay is in stark contrast with the exponential decay found in conventional photonic band-gaps. This power-law BS behaviour can be associated to the singular nature of the band-gap around the Weyl point [44, 47]. Importantly, as we discuss below, the topological protection of the Weyl points enables simultaneously a unique feature, that is, the *tunability* of that power-law behaviour.

To illustrate this tunability, we focus now on the situation in which  $M \neq 0$ . The topological protection of Weyl points implies that by tuning  $M \in (-2J, 2J)$ , one can change locally the band structure without opening a band-gap, which only happens at  $|M| \geq \pm 2J$  when two Weyl points of opposite chi-

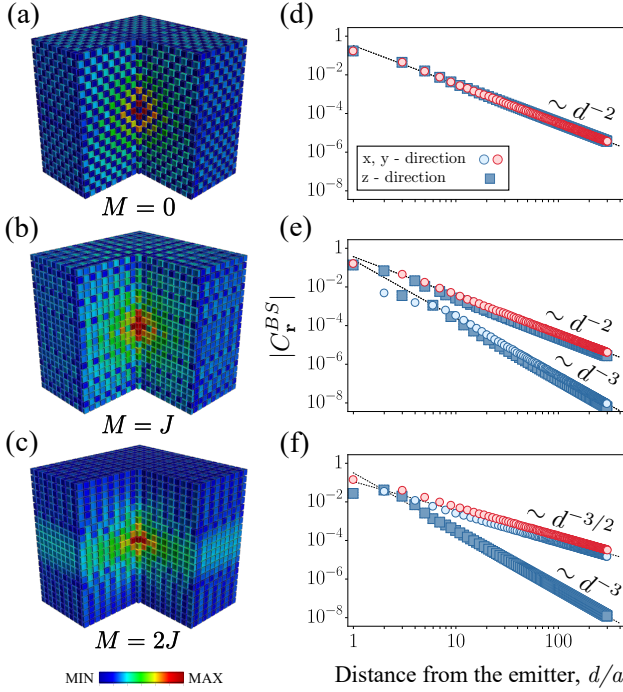


Figure 2. (a), (b), (c): Three-dimensional real-space distribution of the photonic probability amplitudes ( $|C_{\mathbf{r}}^{BS}|$ ) corresponding to the light-matter bound state emerging in the system at long-times for (a)  $M=0$ , (b)  $M=J$  and (c)  $M=2J$ . Blue (red) corresponds to the minimum (maximum) value of  $|C_{\mathbf{r}}^{BS}|$ . Panels (d), (e), and (f) show the calculated dependence of  $|C_{\mathbf{r}}^{BS}|$  along the  $xy$ -directions (circles) and  $z$ -direction (squares), as a function of the distance  $d$  to the quantum emitter for (d)  $M=0$ , (e)  $M=1$  and (f)  $M=2$ . In these panels, blue and red correspond to sublattice  $A$  and  $B$  sites, respectively. The same values for  $g$  and the detunings  $\Delta = \omega_e - \omega_W$  as in Fig. 1 are assumed.

rality meet in  $\mathbf{k}$ -space. Then, while the steady-state population in the spontaneous emission dynamics remains mostly flat (as shown in the inset of Fig. 1(d)), the spatial distribution of the BS that appears at  $E_{BS} = 0$  changes dramatically with  $M$ . Figures 2(b) and (c) (corresponding to  $M=J$  and  $M=2J$ , respectively) show how, as the value of  $M$  grows,  $|C_{\mathbf{r}}^{BS}|$  starts departing from the isotropic distribution found for  $M=0$  and becomes increasingly confined in the  $xy$ -plane. Remarkably, this behavior is reflected in the fact that the power-law exponents governing the spatial decay of  $|C_{\mathbf{r}}^{BS}|$ ,  $1/d^\gamma$ , can actually be varied in the interval  $\gamma \in [3/2, 3]$ , depending on  $M$  and the spatial direction under consideration (see Figs. 2(e) and 2(f)) [48]. The possibility of obtaining different power-law decays in the same photonic platform does not have, up to our knowledge, any counterpart in any other photonic scenario. Furthermore, we expect that the BS will inherit the robustness to disorder of the bath [7, 8], similarly to what occurs in topological photonic waveguides [49].

The physical relevance of these tunable BSs becomes most apparent when many QEs couple to the bath at  $\Delta = 0$ . In that case, as we discuss below, these BSs can mediate decoherence-free emitter interactions. This can be shown ex-

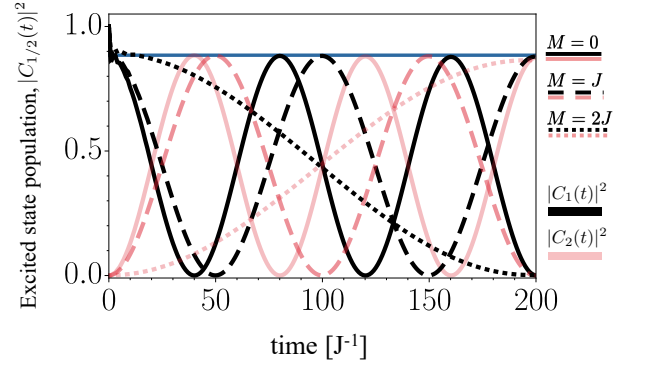


Figure 3. Dynamics of the excited state populations of two emitters ( $|C_1(t)|^2$  and  $|C_2(t)|^2$ , shown in black and pink, respectively), coupled to two different lattice sites with relative position  $\mathbf{r}_2 - \mathbf{r}_1 = a\hat{z}$ . Both emitters feature  $\Delta = 0$  and belong to sublattice  $A$ . The results for three different values of the sublattice energy offset,  $M$ , are shown (solid, dashed and dotted lines correspond to  $M=0$ ,  $M=1$  and  $M=2$ , respectively —the color code of each line defines the emitter to which the corresponding result belongs to). The blue horizontal solid line marks the excited state population of a single emitter in the limit  $t \rightarrow \infty$  for  $M=0$ . In all calculations  $g = 0.5J$  is assumed.

plicitly within a Markovian description of the effective quantum dynamics of the emitters, obtained by tracing out the photonic degrees of freedom [50], and which is governed by the following spin Hamiltonian [43, 51, 52]:

$$H_{\text{spin}} = \sum_{jj'} J_{jj'}^{\alpha\alpha'} \sigma_{eg}^j \sigma_{ge}^{j'}, \quad (2)$$

without any associated dissipative term. In Eq. (2),  $J_{jj'}^{\alpha\alpha'}$  represents the interaction between the pair of emitters  $j$  and  $j'$  ( $\alpha, \alpha' = A/B$  denotes the sublattice to which the corresponding emitter belongs to) and  $\sigma_{\mu\nu}^j$  is the spin-operator of the  $j$ -th QE. The crucial point to realize is that, in the studied system,  $J_{jj'}^{\alpha\alpha'}$  inherits the dependence with the distance between the two emitters ( $|\mathbf{r}_j - \mathbf{r}_{j'}|$ ) from the space dependence of the BS photonic wavefunction, i.e.,  $J_{jj'}^{AA(AB)} \propto C_{\mathbf{r}_j - \mathbf{r}_{j'}}^{BS}$  [43]. This, in turn, allows Weyl photons to mediate decoherence-free, long-range, tunable interactions between the emitters. To prove it numerically, Fig. 3 shows the dynamics of the excited state population associated to two emitters (labeled as 1 and 2) coupled to two different  $A$ -sites of the Weyl lattice (such that  $\mathbf{r}_2 - \mathbf{r}_1 = a\hat{z}$ ). As seen, we obtain the signature of the above described interactions, that is, the reversible exchange of excitations between the two emitters when one of them is initially excited and the other one is in the ground state. In particular, Fig. 3 shows that a long-lived coherent exchange of excitations takes place between the QEs for the three considered values of  $M$  ( $M=0$ ,  $M=J$  and  $M=2J$ , shown as solid, dashed and dotted lines, respectively). Note that, since Fig. 3 corresponds to exact calculations of the dynamics, the observed oscillations are not complete, reaching a maximal value coinciding with the steady state population  $|C_e(t \rightarrow \infty)|^2$  shown in Fig. 1(d) (marked by a blue horizontal line in Fig. 3).

Finally, to reveal whether the interactions  $J_{jj'}^{\alpha\alpha'}$  also inherit

the topological structure of the Weyl photonic bath through the BS wavefunction, we computed the associated dispersion of the single-particle sector of  $H_{\text{spin}}$  as a function of the number of neighbours included in the hopping model (which we quantified through the distance  $s$  of the farthest neighbour from any given emitter). Figures 4(a), 4(b), and 4(c) display the calculated dispersions along  $k_z$  (assuming  $k_x a = \pi/2$  and  $k_y = 0$ ) for  $M = 0$ ,  $M = J$  and  $M = 2J$ , respectively. In the three cases, we observe that indeed, due to the long range of the interactions, the dispersion is rather sensitive to  $s$  (we expect convergence with  $s$  by including enough terms in  $H_{\text{spin}}$ ). Both for  $M = 0$  and  $M = J$  we see an apparent crossing between the bands, whose location rapidly converges with  $s$  (no band crossing is observed for  $M = 2J$  [53]). By analyzing the dispersion in all  $k$ -directions around these crossings, we found that they are actually Weyl points. This is corroborated by the distribution of the Berry curvature in the vicinity of these degeneration points. Figures 4(d) and 4(e) display a cross-section of the Berry curvature [54] along the  $\{k_x, k_z\}$  plane (with  $k_y = 0$ ), calculated for largest value of  $s$  ( $s/a = 9$ ) considered in Figs. 4(a) and 4(b), respectively. The topological character of the Weyl points (magenta circles) as sources or drains of Berry curvature is clearly visualized (for comparison, Fig. 4(f) shows the results  $M = 2J$ , in which no Weyl points are present). Thus, we conclude that the non-interacting part of the effective spin Hamiltonian indeed inherits the non-trivial topological properties of the underlying photonic bath.

In conclusion, we have studied the quantum optical consequences of letting quantum emitters interact through Weyl photons. Using an exact formalism, we have uncovered several distinctive features of the individual and collective quantum emitter dynamics induced by these type of photons. Among these features, the generation of decoherence-free, tunable, long-range interactions obtained by exploiting the topological properties of Weyl points stands out as the most important result of this Letter, with potential applications in quantum information and simulation. Beyond the particular realization reported here, we believe that the concept of using topological protected points to enable tunable long-range interactions could be exported to other setups to find different power-law behaviours, and could stimulate further research of novel quantum optical phenomena in other topological photonic setups.

We acknowledge financial support from the Spanish MINECO under grant MAT2015-66128-R, grant RTI2018-098452-B-I00 (MCIU/AEI/FEDER, UE) and the “María de Maeztu” programme for Units of Excellence in R&D (MDM-2014-0377). AGT acknowledges support from CSIC Research Platform on Quantum Technologies PTI-001 and from Spanish project PGC2018-094792-B-I00 (MCIU/AEI/FEDER, EU).

We note that, while completing this manuscript, we found that some of the results reported in an earlier version of this manuscript [55] were also recently reported by L. Ying *et al.* [56].

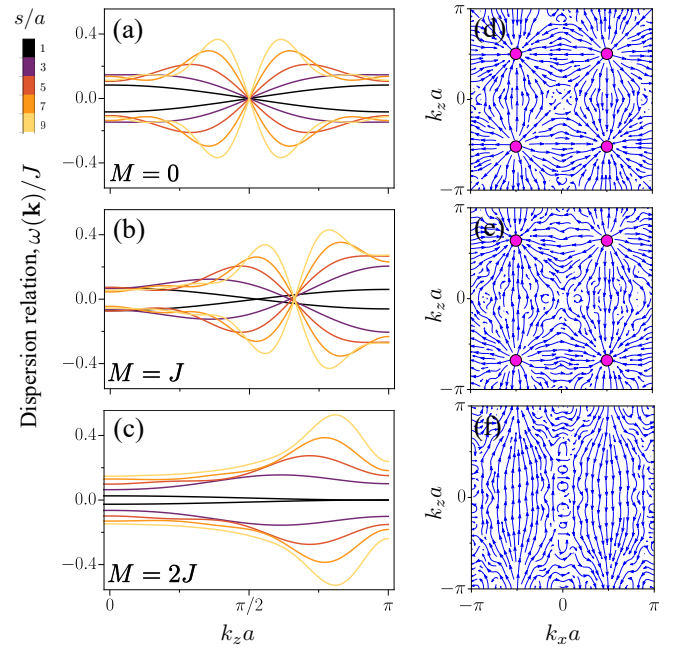


Figure 4. (a), (b), and (c): Dispersion relation along  $k_z$  (with  $k_x a = \pi/2$  and  $k_y = 0$ ) corresponding to the effective spin Hamiltonian discussed in the main text for  $M = 0$ ,  $M = J$ , and  $M = 2J$ , respectively. Results for different values of the distance ( $s$ ) of the farthest neighbor included in the effective model are shown. The color gradient (from dark to light) denotes increasing values of  $s/a$  in the set  $s/a = 1, 3, 5, 7, 9$ . (d), (e), and (f): Berry curvature in the  $k_y = 0$  plane corresponding to the bands in (a), (b) and (c), respectively, as computed for the case  $s/a = 9$ . In panels (d) and (e) the positions of the Weyl points are indicated by magenta circles.

\* a.gonzalez.tudela@csic.es

† jorge.bravo@uam.es

- [1] L. Lu, J. D. Joannopoulos, and M. Soljačić, Nat. Phot. **8**, 821 (2014).
- [2] T. Ozawa, H. M. Price, A. Amo, N. Goldman, M. Hafezi, L. Lu, M. Rechtsman, D. Schuster, J. Simon, O. Zilberberg, and I. Carusotto, Rev. Mod. Phys. **91**, 015006 (2019).
- [3] M. S. Rider, S. J. Palmer, S. R. Pockock, X. Xiao, P. A. Huidobro, and V. Giannini, J. Appl. Phys. **125**, 120901 (2019).
- [4] H. Weyl, Z. Phys. **56**, 330 (1929).
- [5] A. H. Castro Neto, F. Guinea, N. M. R. Peres, K. S. Novoselov, and A. K. Geim, Rev. Mod. Phys. **81**, 109 (2009).
- [6] N. P. Armitage, E. J. Mele, and A. Vishwanath, Rev. Mod. Phys. **90**, 015001 (2018).
- [7] M. Buchhold, S. Diehl, and A. Altland, Phys. Rev. B **98**, 205134 (2018).
- [8] M. Buchhold, S. Diehl, and A. Altland, Phys. Rev. Lett. **121**, 215301 (2018).
- [9] L. Lu, Z. Wang, D. Ye, L. Ran, L. Fu, J. D. Joannopoulos, and M. Soljačić, Science **349**, 622 (2015).
- [10] T. Dubček, C. J. Kennedy, L. Lu, W. Ketterle, M. Soljačić, and H. Buljan, Phys. Rev. Lett. **114**, 225301 (2015).
- [11] J. Bravo-Abad, L. Lu, L. Fu, H. Buljan, and M. Soljačić, 2D Materials **2**, 034013 (2015).
- [12] M. Xiao, Q. Lin, and S. Fan, Phys. Rev. Lett. **117**, 057401



- (2016).
- [13] Q. Lin, M. Xiao, L. Yuan, and S. Fan, Nat. Comm. **7**, 13731 (2016).
  - [14] W.-J. Chen, M. Xiao, and C. T. Chan, Nat. Comm. **7**, 13038 EP (2016).
  - [15] W. Gao, B. Yang, M. Lawrence, F. Fang, B. Béri, and S. Zhang, Nat. Comm. **7**, 12435 EP (2016).
  - [16] M. Zhou, L. Ying, L. Lu, L. Shi, J. Zi, and Z. Yu, Nat. Comm. **8**, 1388 (2017).
  - [17] J. Noh, S. Huang, D. Leykam, Y. D. Chong, K. P. Chen, and M. C. Rechtsman, Nat. Phys. **13**, 611 (2017).
  - [18] B. Yang, Q. Guo, B. Tremain, L. E. Barr, W. Gao, H. Liu, B. Béri, Y. Xiang, D. Fan, A. P. Hibbins, and S. Zhang, Nat. Comm. **8**, 97 (2017).
  - [19] S. Roy, M. Kolodrubetz, N. Goldman, and A. G. Grushin, 2D Materials **5**, 024001 (2018).
  - [20] B. Yang, Q. Guo, B. Tremain, R. Liu, L. E. Barr, Q. Yan, W. Gao, H. Liu, Y. Xiang, J. Chen, C. Fang, A. Hibbins, L. Lu, and S. Zhang, Science **359**, 1013 (2018).
  - [21] Q. Yan, R. Liu, Z. Yan, B. Liu, H. Chen, Z. Wang, and L. Lu, Nat. Phys. **14**, 461 (2018).
  - [22] M. Fruchart, S.-Y. Jeon, K. Hur, V. Cheianov, U. Wiesner, and V. Vitelli, Proc. Natl. Acad. Sci. U.S.A. **115**, E3655 (2018).
  - [23] H. Jia, R. Zhang, W. Gao, Q. Guo, B. Yang, J. Hu, Y. Bi, Y. Xiang, C. Liu, and S. Zhang, Science **363**, 148 (2019).
  - [24] A. Cerjan, S. Huang, M. Wang, K. P. Chen, Y. Chong, and M. C. Rechtsman, Nat. Phot. (2019), DOI:10.1038/s41566-019-0453-z.
  - [25] S. John and J. Wang, Phys. Rev. Lett. **64**, 2418 (1990).
  - [26] S. John and T. Quang, Phys. Rev. A **50**, 1764 (1994).
  - [27] G. Kurizki, Phys. Rev. A **42**, 2915 (1990).
  - [28] V. P. Bykov, Soviet Journal of Quantum Electronics **4**, 861 (1975).
  - [29] E. Shahmoon and G. Kurizki, Phys. Rev. A **87**, 033831 (2013).
  - [30] E. Shahmoon, P. Grišins, H. P. Stimming, I. Mazets, and G. Kurizki, Optica **3**, 725 (2016).
  - [31] P. Hauke and L. Tagliacozzo, Phys. Rev. Lett. **111**, 207202 (2013).
  - [32] P. Richerme, Z.-X. Gong, A. Lee, C. Senko, J. Smith, M. Foss-Feig, S. Michalakakis, A. V. Gorshkov, and C. Monroe, Nature **511**, 198 (2014).
  - [33] M. F. Maghrebi, Z.-X. Gong, M. Foss-Feig, and A. V. Gorshkov, Phys. Rev. B **93**, 125128 (2016).
  - [34] T. Koffel, M. Lewenstein, and L. Tagliacozzo, Phys. Rev. Lett. **109**, 267203 (2012).
  - [35] D. Vodola, L. Lepori, E. Ercolessi, A. V. Gorshkov, and G. Pupillo, Phys. Rev. Lett. **113**, 156402 (2014).
  - [36] M. Kastner, Phys. Rev. Lett. **106**, 130601 (2011).
  - [37] J. Argüello-Luengo, A. González-Tudela, T. Shi, P. Zoller, and J. I. Cirac, arXiv:1807.09228 (2018).
  - [38] S. Barik, A. Karasahin, C. Flower, T. Cai, H. Miyake, W. DeGottardi, M. Hafezi, and E. Waks, Science **359**, 666 (2018).
  - [39] A. Blanco-Redondo, B. Bell, D. Oren, B. J. Eggleton, and M. Segev, Science **362**, 568 (2018).
  - [40] S. Mittal, E. A. Goldschmidt, and M. Hafezi, Nature **561**, 502 (2018).
  - [41] T. Dubček, C. J. Kennedy, L. Lu, W. Ketterle, M. Soljačić, and H. Buljan, Phys. Rev. Lett. **114**, 225301 (2015).
  - [42] S. Roy, M. Kolodrubetz, N. Goldman, and A. G. Grushin, 2D Materials **5**, 024001 (2018).
  - [43] See details in Supplementary Material.
  - [44] A. González-Tudela and J. I. Cirac, Quantum **2**, 97 (2018).
  - [45] In  $H_I$  we assume that the QE couples locally to a single photonic mode. In all results shown in this work, we assume the QE is coupled to an  $A$  lattice site —similar results were obtained when the QE couples to the  $B$  sublattice.
  - [46] C. Cohen-Tannoudji, J. Dupont-Roc, G. Grynberg, and P. Thickstun, *Atom-photon interactions: basic processes and applications* (Wiley Online Library, 1992).
  - [47] A. González-Tudela and J. I. Cirac, Phys. Rev. A **97**, 043831 (2018).
  - [48] One subtlety here is that in order to find the BS energy at zero, one needs to set the detuning of the emitter at a  $\Delta_c \neq 0$  —see [43] for further details on  $\Delta_c$ .
  - [49] M. Bello, G. Platero, J. I. Cirac, and A. González-Tudela, arXiv:1811.04390 (2018).
  - [50] Although the Born-Markov approximation can be seen as not strictly valid in the regime studied in this work, we expect it to be a good approximation when  $g \ll J$ , as it also happens with the single QE behavior.
  - [51] J. S. Douglas, H. Habibian, C.-L. Hung, A. Gorshkov, H. J. Kimble, and D. E. Chang, Nature Photonics **9**, 326 (2015).
  - [52] A. González-Tudela, C.-L. Hung, D. E. Chang, J. I. Cirac, and H. Kimble, Nature Photonics **9**, 320 (2015).
  - [53] This fact can be ascribed to the highly anisotropic nature of BS distribution for  $M = 2J$ , which could make it necessary the inclusion of more neighbour interactions in the  $xy$  plane.
  - [54] M. V. Berry, Proc. Roy. Soc. Lon., Ser. A **392**, 45 (1984).
  - [55] I. Garcia-Elcano, A. Gonzalez-Tudela, and J. Bravo-Abad, arXiv:1903.07513 (2019).
  - [56] L. Ying, M. Zhou, M. Mattei, B. Liu, P. Campagnola, R. H. Goldsmith, and Z. Yu, arXiv:1906.08389 (2019).